Syntheses, Crystal and Electronic Structures, and Linear Optics of $LiMBO_3$ (M = Sr, Ba) Orthoborates

W.-D. Cheng,* H. Zhang, Q.-S. Lin, F.-K. Zheng, and J.-T. Chen

Fujian Institute of Research on the Structure of Matter, Chinese Academy of Sciences, State Key Laboratory of Structural Chemistry, Fuzhou, Fujian 350002, People's Republic of China

Received October 10, 2000. Revised Manuscript Received March 7, 2001

The syntheses, crystal and electronic structures, and linear optical properties of the new orthoborates $LiMBO_3$ (M = Sr, Ba) are reported here. These compounds, which crystallize in the monoclinic space group $P2_1/n$ with cell dimensions a = 6.476(2), b = 6.684(3), c = 6.843(3) Å, β = 109.41(3)°, and Z = 4 for M = Sr, a = 6.372(1), b = 7.022(3), c = 7.058(1) Å, β = 113.89(1)°, and Z = 4 for M = Ba, are modeled in terms of the cluster units $(LiMBO_3)_2$. The calculated electronic structures show that the top of the valence band consists of mostly the O 2p orbitals and the bottom of the conduction band consists of cationic orbitals. The dynamic refractive indices of these orthoborates are obtained in the framework of the INDO/SCI approximation together with the "sum-over-states" method. It is found that the refractive index is larger for $LiSrBO_3$ than for $LiBaBO_3$ and the charge transfer from O^{2-} anionic orbitals to cationic orbitals appears to provide significant contribution to the linear polarizability of these compounds.

1. Introduction

Research efforts have been directed at solid-state borates due to a variety of physical and chemical features exhibited by these compounds, such as luminescence of doped borates SrB_4O_7[1,2] and $X_2Z(BO_3)_2$ (X = Ba, Sr, Ca; Z = Ca, Mg),[3] nonlinear optical properties[4] of borate compounds including the $(B_3O_6)^{3-}$ group, and catalytic activity of the zinc−copper borate $ZnCu_2(BO_3)_2$.[5] Among nonlinear optical crystals, solid-state borates have emerged as the pre-eminent materials for high-power applications, and now, they are being utilized in the manufacture of components in essentially all complex microprocessor-based devices from PCs to cellular phones. An understanding of the relationship between microscopic structure and macroscopic properties has been recognized as an important aid in the design and improvement of materials.[6] Cheng et al. have calculated the electronic structures and nonlinear optical coefficients of MB_6O_{10} (M = Cs_2, Li_2, CsLi) with an aim to understand the electronic origin of their optical susceptibility.[7] Keszler and co-workers have systematically investigated the syntheses, structures, and properties of alkali-metal borates searching for a trend in the structure−property relationship.[8,9]

In this study, we first report the syntheses and single-crystal structural determinations for mixed alkaline and alkaline-earth metal orthoborates $LiMBO_3$ (M = Sr, Ba), and we find that the structural types of our obtained compounds are different from those of the $LiABO_3$ orthoborates (A = Mg, Mn, Co, Zn, and Cd) reported in references.[10−13] Belkebir and co-workers have calculated the crystallographic cell of the phases of $LiZnBO_3$ obtained by solid-state reaction without melting by indexing their X-ray power diffraction patterns, and the two structures found are monoclinic probably with the same Li−Zn cationic disorder as evidenced by vibrational behavior.[13] Piffard and co-workers have determined the structure of $LiCoBO_3$ to be of the space group $C2/c$ and indicated that the Co and Zn cations have occupied similar positions within the trigonal bipyramids above and below the center plane in $LiCoBO_3$ and $LiZnBO_3$, respectively.[10] Then, we use a cluster unit representing the crystalline orthoborate lattice to calculate the electronic structure and refractive indices of mixed alkaline-earth metal and lithium orthoborates $LiMBO_3$ (M = Sr, Ba). In this way, we obtain a means to examine structural and compositional contributions to linear optical properties. The calculated results show a larger refractive index for $LiSrBO_3$ than for $LiBaBO_3$ and indicate that the charge transfers from O 2p orbitals to cation valence orbitals have major contributions to the refractive indices of $LiMBO_3$ (M = Sr, Ba).

* To whom correspondence should be addressed.

(1) Blasse, G.; Dirksen, G. J.; Meijerink, A. *Chem. Phys. Lett.* **1990**, *167*, 41−44.
(2) Meijerink, A.; Nuyten, J.; Blasse, G. *J. Lumin.* **1989**, *44*, 19−31.
(3) Verstegen, J. M. P. J. *J. Electrochem. Soc. Solid-State Sci. Technol.* **1974**, *121*, 1631−1633.
(4) Chen, C.-Z.; Gao, D.-S.; Chen, C.-T. *Acad. Thesis Conf. Cryst. Growth Mater. (China)* **1979**, *B44*, 107−111.
(5) Zletz, A. U.S. Patent Application, 709, 790, March 11, 1985, Amoco Corp.
(6) Munowitz, M.; Jarman, R. H.; Harrison, J. F. *Chem. Mater.* **1993**, *5*, 661−671; **1993**, *5*, 1257−1267.
(7) Cheng, W.-D.; Chen, J.-T.; Lin, Q.-S.; Zhang, Q.-E.; Lu, J.-X. *Phys. Rev. B* **1999**, *60*, 11747−11754.
(8) Akella, A.; Keszler, D. A. *J. Solid State Chem.* **1995**, *120*, 74−79.
(9) Smith, R. W.; Keszler, D. A. *J. Solid State Chem.* **1997**, *129*, 184−188.
(10) Piffard, Y.; Rangan, K. K.; An, Y.; Guyomard, D.; Tournoux, M. *Acta Crystallogr.* 1998, *C54*, 1561−1563.
(11) Norrestam, R. *Z. Kristallogr.* **1989**, *187*, 103−110.
(12) Sokolova, E. V.; Simonov, M. A.; Belov, N. V. *Z. Kristallogr.* **1980**, *25*, 1285−1286.
(13) Belkebir, A.; Tarte, P.; Rulmont, A.; Gilbert, B. *New J. Chem.* **1996**, *20*, 311−316.

10.1021/cm000808i CCC: $20.00
Published on Web 04/27/2001

Table 1. Crystal Parameters

formula	$LiSrBO_3$	$LiBaBO_3$
fw	153.37	203.09
space group	*P*2(1)/*n*	*P*2(1)/*n*
a (Å)	6.4800(13)	6.372(1)
b (Å)	6.6800(13)	7.022(3)
c (Å)	6.8400(14)	7.058(1)
β (deg)	109.41(3)	113.89(1)
V (Å^3)	279.25(10)	288.7(2)
Z	4	4
D_{calc} (mg/m^3)	3.648	4.67
R	0.0443	0.0551
Rw	0.0898	0.0626
S	0.982	0.93

2. Experimental and Computational Procedures

2.1. Syntheses and Crystal Growths. 2.1.1. $LiSrBO_3$. A mixture containing appropriate amounts of $LiCO_3$ (Chemical pure), $SrCO_3$ (Chemical pure), and H_3BO_3 (Analytical reagent) was ground into fine powder in a mortar of agate. This mixture was heated to 450 °C in a platinum crucible and kept at this temperature for 4 h, followed by heating at 840 °C for 10 h and at 910 °C for 24 h. The mixture, then, was cooled from 910 to 600 °C at a rate of 2.7 °C h^{-1}. It finally was quenched to room temperature. A few colorless pillar crystals were found from the melt of the mixture.

2.1.2. $LiBaBO_3$. A stoichiometric mixture of $LiCO_3$ (0.74 g, chemical pure), BaF_2 (1. 71 g, analytical reagent), $SrCO_3$ (1.48 g, chemical pure), and H_3BO_3 (1.24 g, analytical reagent) was ground into fine powder in a mortar of agate, then heated to 450 °C in a platinum crucible, and kept at this temperature for 4 h, followed by heating at 840 °C for 24 h and at 910 °C for 24 h, then cooled from 910 to 800 °C at a rate of 1.0 °C h^{-1} and from 800 to 600 °C at a rate of 4.0 °C h^{-1}, and finally air-quenched to room temperature. A few colorless pillar crystals were found from the melt.

2.2. X-ray Determination. A single crystal of $LiSrBO_3$ and $LiBaBO_3$ with approximate dimensions 0.18 × 0.08 × 0.06 and 0.30 × 0.20 × 0.10 mm^3 was selected for single-crystal X-ray diffraction, respectively. The diffraction data were collected on an Enraf-Nonius CAD4 diffractometer with graphite monochromator Mo Kα radiation for these two crystals. Cell constants were obtained from least-squares refinement, using the setting angles of 25 reflections in the range $26° < 2\theta < 48°$ for $LiSrBO_3$ and 25 reflections in the range $22° < 2\theta < 46°$ for $LiBaBO_3$. The crystallographic parameters of these two crystals are listed in Table 1. The intensity data were collected at 273 K in the range $-11 \le h \le 11$, $0 \le k \le 12$, and $0 \le l \le 12$ for $LiSrBO_3$ and the range $0 \le h \le 12$, $0 \le k \le 13$, and $-13 \le l \le 13$ for $LiBaBO_3$, using the $\omega/2\theta$ scan technique with a scan speed of 5°/min and a scan width of $\Delta\omega = (0.8 + 0.35 \tan\theta)°$, respectively. The intensities of three standard reflections were measured every 60 min, and the intensity decay was 0.6 and 4.7% for crystals $LiSrBO_3$ and $LiBaBO_3$, respectively. Lorentz and polarization corrections were applied to the data. The linear absorption coefficients are 14.3 and 135.3 mm^{-1} for these two crystals, respectively. An empirical absorption correction based on a ψ-scan was applied and the relative transmission coefficients ranged from 0.324 to 1.00 with an average value of 0.662 and from 0.484 to 0.996 with an average value of 0.740, respectively. The 1824 and 2301 reflections were used to measured with $2\theta_{max} = 80°$; 1223 and 1490 reflections with $I > 3\sigma(I)$ were used in structural determination and refinement for $LiSrBO_3$ and $LiBaBO_3$ crystals, respectively.

The structures of $LiSrBO_3$ and $LiBaBO_3$ were separately determined by the Shelx/PC and MolEN/PC programs. From the systematic absence of *h*0*l*: $l = 2n$; *0k*0: $k = 2n$ and from subsequent least-squares refinement, the space group of these two crystals was determined to be $P2_1/n$. Note that this space group is not a standard space group. However, it is often convenient and the angle of β will not become much larger than 90° when we prefer the space group $P2_1/n$ in determining the crystal structures. The Sr and Ba atoms were located from the direct method; the remaining atoms were located in succeeding difference Fourier synthesis. The final full-matrix least-squares refinement for 56 and 55 variable parameters converged to $R = 4.43\%$, $Rw = 8.98\%$ [in which $w = 1/(\sigma^2(F_o^2) + (aP)^2 + bP)$; $P = (2F_c^2 + \mathrm{Max}(F_o^2,0))/3$], $S = 0.982$, and $(\Delta/\sigma)_{max} = 0.0001$ for $LiSrBO_3$ and converged to $R = 5.51\%$, $Rw = 6.26\%$ [in which $w = 1/(\sigma^2(F) + (0.020F)^2 + 1.0)$], $S = 0.93$, and $(\Delta/\sigma)_{max} = 0.0001$ for $LiBaBO_3$. Neutral atomic scattering factors were taken from Cromer and Waber.[14] The maximum and minimum peaks on the final different Fourier map are 1.43 and −1.00 e/Å^3 and 5.57 and −1.72 e/Å^3 for $SrLiBO_3$ and $BaLiBO_3$ crystals, respectively. The atom coordinates and thermal parameters are listed in Table 2. Here, it is noted that the BaF_2 attempted as a flux was added into the mixture of $SrCO_3$, $LiCO_3$, and H_3BO_3, and the variation of temperature was controlled to try and obtain a new phase of $LiSrBO_3$. However, the crystal of $LiBaBO_3$ was found in the X-ray structural determination and the atom of Sr was not present in this crystal. We made a trial structure including the Sr atoms in the $LiBaBO_3$ during the solution of crystal structure by the Shelxtl/PC program. The result showed a large value of *R* and unreasonable coordinations of metal atoms. Accordingly, we believe no Sr atoms are in this crystal structure.

Table 2. Fractional Atomic Coordinates and Equivalent Isotropic Displacement Parameters (Å)

atom	*x*	*y*	*Z*	U_{eq}[a]
		$LiSrBO_3$		
Sr	0.20197(5)	0.12378(5)	0.86760(5)	0.00811(9)
O(1)	0.1560(5)	0.1105(4)	1.2178(4)	0.0130(5)
O(2)	0.1073(5)	0.2993(4)	0.4940(4)	0.0109(4)
O(3)	0.1963(5)	0.4897(4)	0.9367(4)	0.0109(5)
B	0.1886(6)	0.1326(6)	0.4270(6)	0.0084(5)
Li	0.1002(13)	0.4086(10)	1.1930(11)	0.0136(13)
		$LiBaBO_3$		
Ba	0.33502(8)	0.13980(7)	0.15907(6)	0.01093(6)
O(1)	0.3793(9)	0.3180(7)	0.5164(8)	0.0085(9)
O(2)	0.291(1)	0.1598(9)	0.7740(8)	0.017(1)
O(3)	0.2199(9)	0.0011(7)	0.4569(7)	0.0074(9)
B	0.296(1)	0.160(1)	0.579(1)	0.007(1)
Li	0.896(2)	0.071(2)	0.298(2)	0.009(3)

[a] $U_{eq} = {}^1/_3\sum_i\sum_j U^{ij}\alpha_i^*\alpha_j^* a_i a_j$.

2.3. Computational Details. The wave functions and energies obtained from electronic structural calculations were employed to compute the polarizabilities of clusters, and the electronic structural calculations of the clusters were based on an all-valence-electron, semiempirical INDO self-consistent field (SCF) molecular orbital (MO) procedure with configuration interaction (CI) modified by Zerner and co-workers.[15−18] There are the one-center core integral $U_{\mu\mu}$, resonance integral $\beta_{\mu\nu}$, two-electron integral $\gamma_{\mu\nu}$, overlap integral $S_{\mu\nu}$, and density matrix element $\mathbf{P}_{\mu\nu}$ in the matrix element of the Fock operator under the INDO approximation. The INDO model as employed herein included all one-center two-electron integrals and two-center two-electron integrals $\gamma_{\mu\nu}$. The one-center two-electron integrals $\gamma_{\mu\mu}$ were chosen from the Pariser approximation, $\gamma_{\mu\mu} = F^0(\mu\mu) = \mathrm{IP}_\mu - \mathrm{EA}_\mu$, and the two-center two electron integrals were calculated using the Mataga−Nishimoto formula, $\gamma_{\mu\nu} = 1.2/[R_{AB} + 2.4/(\gamma_{\mu\mu} + \gamma_{\nu\nu})]$ in the spectroscopic version of the INDO method. The Slater orbital exponents ζ and the other calculating parameters are listed in Table 3. The molecular orbital calculations were performed by the restricted Hartree−Fock method. The ground state was constructed as a single

(14) Cromer, D. T.; Waber, J. T. In *International Table for X-ray Crystallography*; Kynoch Press: Birmingham, 1974; Vol. IV, Table 2.2A, p 71.

(15) Bacon, A. D.; Zerner, M. C. *Theor. Chim. Acta* **1979**, *53*, 21−54.

(16) Zerner, M. C.; Lovw, G. H.; Kirchner, R. F.; Mueller-Westerhoff, U. T. *J. Am. Chem. Soc.* **1980**, *102*, 589−599.

(17) Anderson, W. P.; Edwards, E. D.; Zerner, M. C. *Inorg. Chem.* **1986**, *25*, 2728−2732.

(18) Anderson, W. P.; Cundari, T. R.; Zerner, M. C. *Int. J. Quantum Chem.* **1991**, *39*, 31−45.

Table 3. INDO/S Model Parameters

parameter	B	O	Li	Sr	Ba
$\zeta_{ns,np}$ (Å^{-1})	1.300	2.275	0.650	1.214	1.263
$\zeta_{(n-1)d}$ (Å^{-1})				2.058	2.658
$-I_{ns}$ (eV)	14.05	32.90	5.41	5.84	5.21
$-I_{np}$ (eV)	8.70	17.28	3.61	3.76	3.43
$-I_{(n-1)d}$ (eV)				3.66	3.22
$-\beta_{ns,np}$ (eV)	17.00	34.20	9.00	1.88	2.66
$-\beta_{(n-1)d}$ (eV)				10.05	12.50
$\gamma_{ns,np}$ (eV)	8.68	13.00	4.57	3.75	4.68
$\gamma_{(n-1)dd}$ (eV)				5.31	5.19
$\gamma_{(n-1)dns,np}$				4.53	3.79

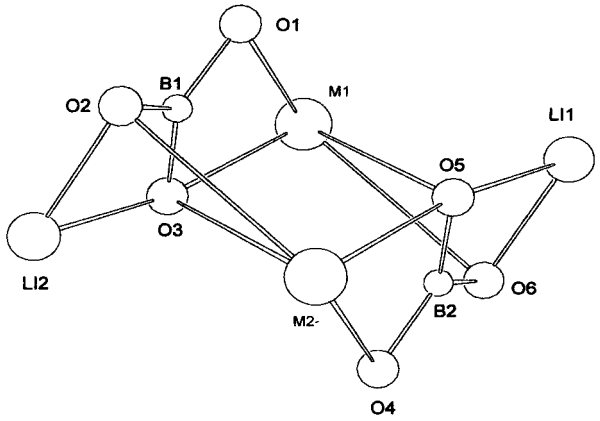

Figure 1. Selected cluster unit model of ($LiMBO_3$).

determinant from the Hartree−Fock SCF calculated results. Only single-substituted determinants relative to the ground state configuration were considered and only singlet spin-adapted configurations needed to be included in the CI calculations. The ground state and all excited states had the multiplicity of 1. The electron was promoted from the 13 highest occupied orbitals to the 13 lowest unoccupied orbitals and the configuration space was constructed by these 26 active orbitals. The wave functions and energy eigenvalues of the excited states were determined by solving the secular equation relating to configuration coefficients. The dipole and transition moment matrix elements were expressed as a sum of one-electron integrals.

The cluster units $(LiSrBO_3)_2$ and $(LiBaBO_3)_2$ representing extended oxide crystals $LiSrBO_3$ and $LiBaBO_3$ were selected for calculations, as shown in Figure 1. The coordinate systems are defined in the calculations. The coordinate center is located at the center of the ring [M1M2O3O5]. The *x* axis is defined to be parallel to the connecting line between the O3 and O5 atoms, and the *y* axis is lain down the plane constructed by three atoms, O3−O5−M1 in Figure 1. The *z* axis is defined as the right-hand rule of the coordinate system for these two clusters, respectively. Theoretical calculations of electronic structures and polarizabilities are based on the crystallographic structural data for these two clusters.

The tensor components of the polarizability $\alpha(\omega)$ with frequency dependence for the clusters $(LiSrBO_3)_2$ and $(LiBaBO_3)_2$ were calculated by the sum-over-states (SOS) method as follows:

$$\alpha_{ij}(\omega) = 1/\hbar\Sigma_{m}\mu_{gm}{}^{i}\mu_{mg}{}^{j}[(\omega_{mg} - \omega_{p})^{-1} + (\omega_{mg} + \omega_{p})^{-1}] \quad (1)$$

3. Results and Discussions

3.1. Crystal Structures. Drawings of the contents of the unit cells of compounds $LiMBO_3$ (M = Sr, Ba) are shown in Figure 2. It is found that $LiMBO_3$ structures can be constructed from a stack of [MO] and [LiO] layers along the [10$\bar{1}$] direction and B atoms localized in adjacent layers as a bridging role. In the [LiO] layers, the adjacent polyhedrons constructed from

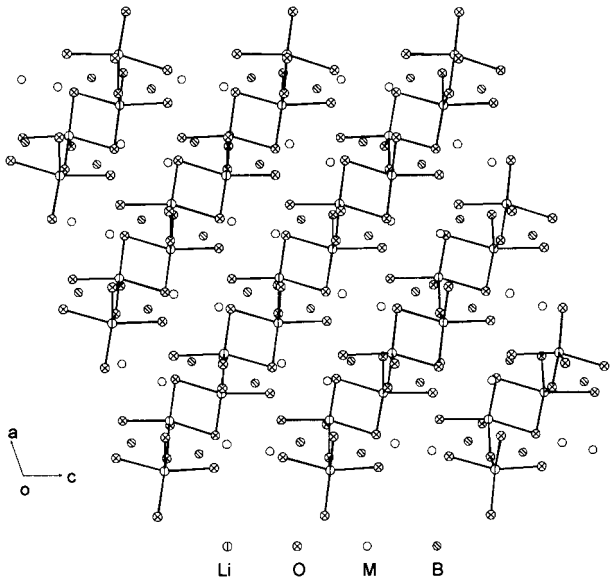

Figure 2. Crystal structure stacked from the [MO] and [101] direction in [$LiMBO_3$]. The M−O bonds are omitted for clarity.

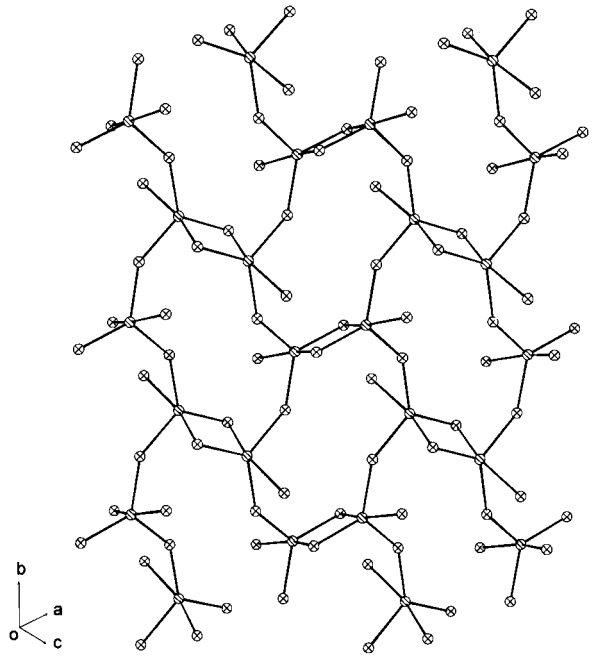

Figure 3. Structure of the [LiO] layer along the *ac* diagonal plane in [$LiMBO_3$].

the LiO_5 form dimers by sharing edges, and each dimer connects with the four adjacent dimers by the four O atoms to form two-dimensional sheets along the *ac* diagonal plane, as shown in Figure 3. The Li atoms are coordinated by five O atoms and the LiO_5 polyhedron is a distorted trigonal bipyramid. For the $LiSrBO_3$ crystal, the Li−O distances vary from 1.955(7) to 2.169(8) Å with an average value of 2.056 Å, where the long bond lengths of Li−O are in the axial direction of the trigonal bipyramid. An average bond length of the Li−O in the $LiBaBO_3$ crystal is close to that of the $LiSrBO_3$ one. The B−O distances vary from 1.369(4) to 1.385(6) Å with an average value of 1.377 Å and the O−B−O angles are between 118.3(7)° and 122.6(7)°. These values are normal in a [BO_3] plane of $LiMBO_3$ (M = Sr, Ba). Table 4 lists the interatomic distances and angles of $LiMBO_3$. There are different coordinations

Table 4. Interatomic Distances (Å) and Bond Angles (deg)

Interatomic Distances (Å)		Bond Angles (deg)		Interatomic Distances (Å)		Bond Angles (deg)	
a. $LiSrBO_3$				**b. $LiBaBO_3$**			
Sr−O(1)	2.6928(7)	O(1)−Sr−O(1)	79.57(2)	Ba−O(1)	2.726(6)	O(1)−Ba−O(1)	131.2(2)
Sr−O(1)	2.513(1)	O(1)−Sr−O(2)	98.01(2)	Ba−O(1)	2.670(6)	O(1)−Ba−O(1)	89.3(2)
Sr−O(2)	2.689(1)	O(1)−Sr−O(2)	82.02(3)	Ba−O(1)	2.677(5)	O(1)−Ba−O(2)	149.6(2)
Sr−O(2)	2.5171(9)	O(1)−Sr−O(2)	155.856(9)	Ba−O(2)	2.622(6)	O(1)−Ba−O(2)	112.9(1)
Sr−O(2)	2.5297(8)	O(1)−Sr−O(3)	123.03(2)	Ba−O(2)	3.067(8)	O(1)−Ba−O(2)	79.1(2)
Sr−O(3)	2.495(1)	O(1)−Sr−O(3)	93.19(2)	Ba−O(2)	3.030(8)	O(1)−Ba−O(3)	53.0(2)
Sr−O(3)	2.5469(9)	O(1)−Sr−O(2)	149.26(1)	Ba−O(3)	2.675(6)	O(1)−Ba−O(3)	78.3(2)
Li−O(1)	2.0219(9)	O(1)−Sr−O(2)	79.05(1)	Ba−O(3)	2.646(5)	O(1)−Ba−O(3)	68.4(2)
Li−O(1)	2.0131(5)	O(1)−Sr−O(2)	96.83(2)	Ba−O(3)	3.185(5)	O(1)−Ba−O(1)	69.3(2)
Li−O(2)	2.1664(9)	O(1)−Sr−O(3)	80.857(8)	B−O(1)	1.38(1)	O(1)−Ba−O(2)	75.2(2)
Li−O(3)	2.1250(7)	O(1)−Sr−O(3)	155.81(1)	B−O(2)	1.39(1)	O(1)−Ba−O(2)	73.2(2)
Li−O(3)	1.9544(6)	O(2)−Sr−O(2)	131.318(9)	B−O(3)	1.373(8)	O(1)−Ba−O(2)	140.5(2)
B−O(1)	1.3850(6)	O(2)−Sr−O(2)	96.91(2)	Li−O(1)	2.10(2)	O(1)−Ba−O(3)	78.8(2)
B−O(2)	1.3737(4)	O(2)−Sr−O(3)	74.89(2)	Li−O(2)	1.95(2)	O(1)−Ba−O(3)	133.6(1)
B−O(3)	1.3685(4)	O(2)−Sr−O(3)	54.24(3)	Li−O(2)	1.99(2)	O(1)−Ba−O(3)	104.1(2)
		O(2)−Sr−O(2)	73.87(2)	Li−O(3)	1.97(1)	O(1)−Ba−O(2)	87.8(2)
		O(2)−Sr−O(3)	144.00(2)	Li−O(3)	2.20(2)	O(1)−Ba−O(2)	142.2(2)
		O(2)−Sr−O(3)	77.09(2)			O(1)−Ba−O(2)	145.7(2)
		O(2)−Sr−O(3)	79.276(8)			O(1)−Ba−O(3)	74.6(2)
		O(2)−Sr−O(3)	80.34(2)			O(1)−Ba−O(3)	77.9(2)
		O(3)−Sr−O(3)	121.599(5)			O(1)−Ba−O(3)	144.2(2)
		O(1)−Li−O(1)	122.33(2)			O(2)−Ba−O(2)	86.9(2)
		O(1)−Li−O(2)	69.31(1)			O(2)−Ba−O(2)	86.5(2)
		O(1)−Li−O(3)	103.092(9)			O(2)−Ba−O(3)	152.5(2)
		O(1)−Li−O(3)	120.218(5)			O(2)−Ba−O(3)	71.5(2)
		O(1)−Li−O(2)	99.92(2)			O(2)−Ba−O(3)	125.7(2)
		O(1)−Li−O(3)	69.94(2)			O(2)−Ba−O(2)	71.1(2)
		O(1)−Li−O(3)	117.29(3)			O(2)−Ba−O(3)	94.1(2)
		O(2)−Li−O(3)	162.187(8)			O(2)−Ba−O(3)	134.7(2)
		O(2)−Li−O(3)	105.13(2)			O(2)−Ba−O(3)	44.6(2)
		O(3)−Li−O(3)	92.63(2)			O(2)−Ba−O(3)	119.8(1)
		O(1)−B−O(2)	119.62(1)			O(2)−Ba−O(3)	68.3(2)
		O(1)−B−O(3)	119.07(2)			O(2)−Ba−O(3)	59.3(1)
		O(2)−B−O(3)	121.31(3)			O(3)−Ba−O(3)	123.3(2)
						O(3)−Ba−O(3)	69.6(2)
						O(3)−Ba−O(3)	121.5(2)
						O(1)−B−O(2)	119.0(6)
						O(1)−B−O(3)	122.6(7)
						O(2)−B−O(3)	118.3(7)
						O(1)−Li−O(2)	105.8(6)
						O(1)−Li−O(2)	71.3(5)
						O(1)−Li−O(3)	105.8(8)
						O(1)−Li−O(3)	158.0(7)
						O(2)−Li−O(2)	128.1(8)
						O(2)−Li−O(3)	109.3(7)
						O(2)−Li−O(3)	69.4(6)
						O(2)−Li−O(3)	121.5(7)
						O(2)−Li−O(3)	94.5(7)
						O(3)−Li−O(3)	95.9(6)

between the Sr and Ba atoms in $LiMBO_3$ (M = Sr, Ba) crystals. The Sr atoms are coordinated by seven O atoms, and the SrO_7 polyhedron may be described as a mono-capped distorted trigonal prism. The Sr−O distances vary from 2.495(3) to 2.692(3) Å with an average value of 2.594 Å, which compared very well to the expected value 2.590 Å calculated from the crystal radii for the seven-coordinate Sr^{2+} ion.[19] In the [SrO] layers, the Sr atoms through sharing O−O edges extend along the *b* direction to form chains, and the adjacent chains link together by O atoms to form puckering sheets parallel to the *ac* diagonal plane, as shown in Figure 4. These sheets are connected along the [10$\bar{1}$] direction to form the three-dimensional framework by the bridging O atoms of the [LiO] layers. For the $LiBaBO_3$ crystal, however, the Ba atoms are coordinated by nine O atoms and the BaO_9 polyhedron is described as a mono-capped distorted square antiprism. The Ba−O distances vary from 2.622(6) to 3.185(5) Å with an average value of 2.813 Å, which compared well to the expected value 2.850 Å calculated from the crystal radii for the nine-coordinate Ba^{2+} ion.[19] In the [BaO] layers, the Ba atoms through sharing the planes of three oxygen atoms extend along the *ac* diagonal direction to form chains, and the adjacent chains link together by the two oxygen atoms to form puckering sheets in the *b* direction, as shown in Figure 5. These sheets are connected along the [10$\bar{1}$] direction to form the three-dimensional framework by the bridging O atoms of the [LiO] layers.

3.2. Electronic Structures. The energy bands for $LiSrBO_3$ and $LiBaBO_3$ are calculated in terms of MO procedures. Note that the top of the valence band of $LiSrBO_3$ and $LiBaBO_3$ is at −7.07 and −5.65 eV, respectively, and is taken to be zero and regarded as a reference in the following discussion.

The dominant contribution to the lower valence band (i.e., −31.5 to −23.5 eV for $LiSrBO_3$, −28.5 to −24.5 eV for $LiBaBO_3$) comes from O 2s orbitals along with a relatively small (<8%) contribution from B 2s orbitals. It is therefore assigned as an s valence band. The upper

(19) Shannon, R. D. *Acta Crystallogr.* **1976**, *A32*, 751−767.

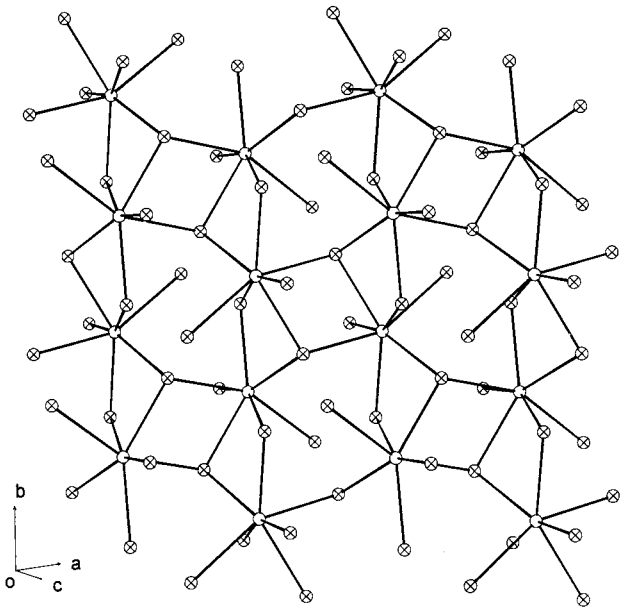

Figure 4. Structure of the [SrO] layer along the *ac* diagonal plane in [$LiSrBO_3$].

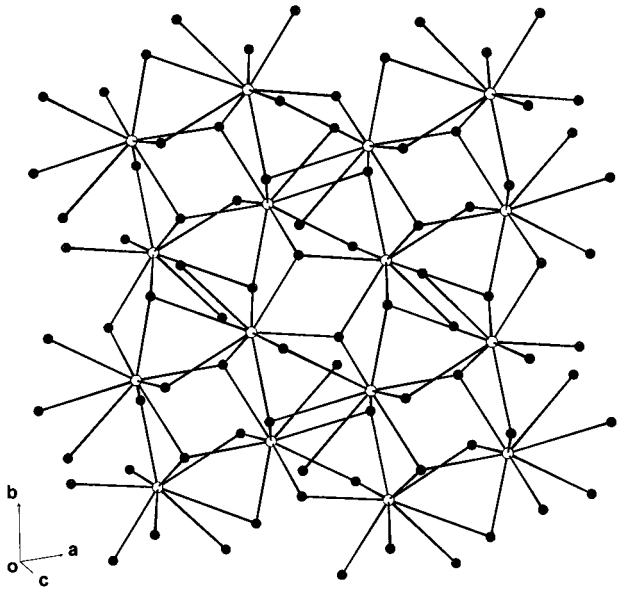

Figure 5. Structure of the [BaO] layer along the *ac* diagonal plane in [$LiBaBO_3$].

valence band ranging from −18.8 to 0.00 eV is a result of contributions from O 2p orbitals that are mixed with B 2p orbitals (less than 37%) for $LiSrBO_3$ and that ranging from −9.5 to 0.00 eV is a result of contributions from O 2p orbitals that are mixed with B 2p orbitals (less than 45%) for $LiBaBO_3$. The atomic state densities of the upper valence bands for $LiSrBO_3$ and $LiBaBO_3$ are displayed in Figure 6a,b, respectively. In Figure 6a, the σ-bonding interactions between the O 2p and B 2p orbitals yield the peaks ranging from −18.8 to −7.0 eV. On the other hand, the peaks localized in the energies from −5.0 to −2.3 eV can be assigned to the π-bonding interactions between the O 2p and B 2p orbitals. Finally, the 2p orbitals of the terminal oxygen atoms dominate the region from −1.9 eV to the top of the valence band. For example, the peak at the energy of −1.7 eV is the contribution from 89% O 2p orbitals. Figure 6a also includes the atomic state density of the lower conduction

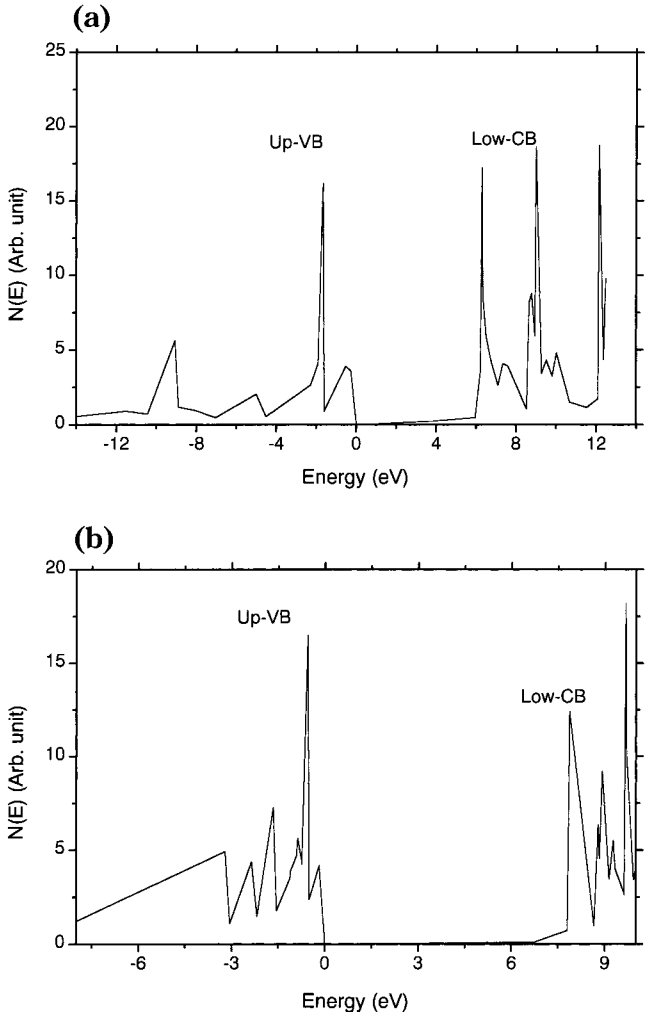

Figure 6. (a) Atomic state density of $LiSrBO_3$. (b) Atomic state density of LiBa BO_3.

band (CB) for $LiSrBO_3$. Here, the peaks localized in the energy region between 3.9 and 13.5 eV are mainly due to contributions from the Sr and Li ionic states. For examples, the band of energy with less than 6.0 eV has contributions of about 58% from the Sr 5s orbital. The three peaks localized at 6.3, 9.0, and 12.1 eV have contributions of about 57% from Sr 4d orbitals and 17% from Sr 5p orbitals, 48% from Sr 4d and 38% from Li 2s orbitals, and 61% from Li 2p orbitals, individually. The conduction band region ranging from 14.1 to 25.0 eV is formed by the antibonding interactions between the orbitals of boron (>60% of 2s and 2p characters) and oxygen (<40% of 2p character), The calculated gap between the top of the valence band and bottom of the conduction band comes out to be 3.86 eV, yielding the absorption edge of the $LiSrBO_3$ crystal to be about 321 nm. In Figure 6b, the σ-bonding interactions between the O 2p and B 2p orbitals contribute in the lowest energy region of the p subband ranging from −9.5 to −3.2 eV. The band from the −3.1 to −1.5 eV is mainly due to the π-bonding interactions between the O 2p and B 2p orbitals. For example, the peak at the energy of −1.7 eV is the contribution from 88% O 2p and 4% B 2p orbitals. The band between the energies −1.1 and 0.0 eV is assigned to the 2p orbitals of the terminal oxygen atoms, and there are contributions of larger than 92% from O 2p orbitals. The three peaks localized at

about the energies of −0.9, −0.6, and −0.2 eV are the contributions of about 97, 95, and 93% from O 2p orbitals. The lower conduction band that ranges from 6.7 to 10.1 eV has contributions from the Ba and Li ionic states. For instance, the highest peak in Figure 6b has the contributions of about 59% from Ba 5d and 12% from Li 2p orbitals. The next band (10.7−15.8 eV) is formed by the antibonding interactions between the boron (>30% of 2s and 2p characters) and oxygen (<46% of 2s and 2p character) orbitals. The minimum energy gap between the top of the valence band and the bottom of the conduction band is calculated to be 6.70 eV, yielding the absorption edge of $LiBaBO_3$ to be about 185 nm.

3.3. Optical Properties. The optical properties of a bulk material can be thought of as being built up from the corresponding properties of individual cluster units or microscopic species. In this approximation, the linear refractive index of frequency dependence can be written as

$$n^2(\omega) = 1 + 4\pi\chi^{(1)}(\omega) \qquad (2)$$

where the linear susceptibility $\chi^{(1)}(\omega)$ is defined as

$$\chi^{(1)}(\omega) = N\alpha(\omega)/[1 - (4\pi/3)N\alpha(\omega)] \qquad (3)$$

Here, $\alpha(\omega)$ is the frequency-dependent polarizability and N is the cluster number density. For the usual case in which the polarizability $\alpha(\omega)$ is positive, we see that the susceptibility is larger than the value $N\alpha(\omega)$ predicted by calculations that ignore local-field corrections. The cluster number density, N, can be obtained by a product of mass density and Avogadro's number that is dividing by molar mass. For $(LiSrBO_3)_2$, with a molecular formula weight of 306.74 g/mol and a mass density of 1.82 g/cm^3, we obtain $N = 3.573 \times 10^{21}$ cm^{-3}. For $(LiBaBO_3)_2$, with a molecular formula weight of 406.18 g/mol and a mass density of 4.67 g/cm^3, we obtain $N = 6.924 \times 10^{21}$ cm^{-3} . It is to be noted here that, through rearrangement of the Lorentz−Lorenz equation, $(\epsilon^{(1)} - 1)/(\epsilon^{(1)} + 2) = 4/3\pi N\alpha$, we can obtain the relationship $(\epsilon^{(1)} + 2)/3 = 1/[1 - (4\pi/3)N\alpha]$.[20] Accordingly, the factor $1/[1 - (4\pi/3)N\alpha]$ or $(\epsilon^{(1)} + 2)/3$ is interpreted as the local-field correction factor for the linear susceptibility and can be described as the interaction between a selected cluster unit and surrounding environment. In fact, the determination of the local field factor can be quite complicated for a condensed system.[21,22] We only take an approximate treatment of a spherical cavity to obtain the local field factor[23] in this study.

Before attempting to compute the frequency dependence of the refractive index for orthoborates $LiSrBO_3$ and $LiBaBO_3$, it is necessary to investigate the convergence behavior in the summation of excited states of clusters $(LiSrBO_3)_2$ and $(LiBaBO_3)_2$. This exercise will help us in determining the reliability of the INDO/SCI method used here. Figure 7 shows the calculated average polarizability $\langle\alpha\rangle$ versus the number of states for these two clusters at 1064 nm. Accordingly, $\langle\alpha\rangle$ is converging very slowly, though it has reached the stability after summation over 150 states, and the convergent behavior is better for the $(LiBaBO_3)_2$ than for the $(LiSrBO_3)_2$. It is well-known that the sum-over-states expansion in eq 1 is, in general, infinite since the applied optical field mixes the ground state to several excited states. Combining the results of Figure 7 with the state density of Figure 6, we can identify that the charge transfers from the O 2p orbitals to metal ionic valence orbitals are the dominant contributors to the calculated linear polarizabilities.

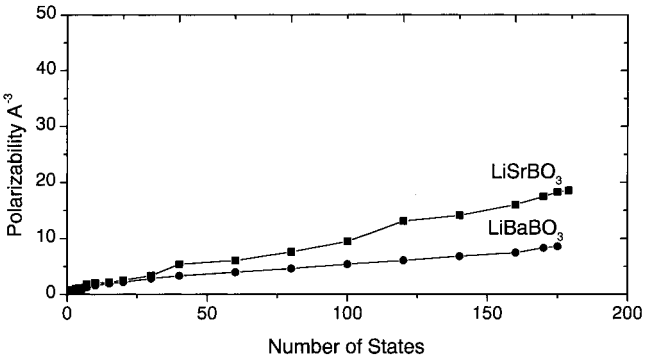

Figure 7. Polarizability $\langle\alpha\rangle$ clusters at 1065 nm.

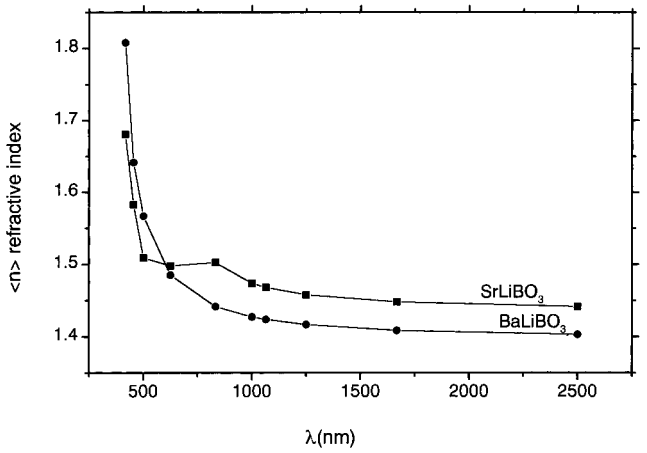

Figure 8. Average refractive index of $SrLiBO_3$ and $BaLiBO_3$ bulks.

The average dynamic refractive index of $\langle n(\omega)\rangle$ was calculated using a general definition for the average polarizability (i.e., $\langle a\rangle = (a_{xx} + a_{yy} + a_{zz})/3$) and eqs 2 and 3. Figure 8 shows the refractive indices $\langle n(\omega)\rangle$ of $LiSrBO_3$ and $LiBaBO_3$ for wavelengths ranging from 350 to 2500 nm. It is found that the dynamic $\langle n\rangle$ is larger for $LiSrBO_3$ than for $LIBaBO_3$ in the low-frequency zone. These are due to a smaller optical gap and larger dipole transition moment for $LiSrBO_3$ than for $LiBaBO_3$. For example, the calculated dipole transition moments of the first two low-lying excited states are 1.47 and 0.96 D for M = Sr and 0.95 and 0.18 D for M = Ba in the $(LiMBO_3)_2$ clusters. It also notes here that calculations of polarizabilities depend on the dipole transition moments, which in fact, depend on the state function and spatial configuration for $LiMBO_3$. At a wavelength of 1.065 μm, the calculated refractive indices, n_x, n_y, and n_z, are individually 1.574, 1.680, and 1.198, and the average $\langle n\rangle$ is 1.484 for $SrLiBO_3$; n_x, n_y, and n_z are individually 1.324, 1.571, and 1.388, and the average $\langle n\rangle$ is 1.428 for $LiBaBO_3$. The refractive indices of these

(20) Boyd, R. W. *Nolinear Optics*; Academic Press: San Diego, CA, 1992; p 148.
(21) Munn, R. *Int. J. Quantum Chem.* **1992**, *43*, 159−169.
(22) Sylvester-Hvid, K. D.; Mikkelsen, K. V.; Patrick, D. J.; Agren, H. J. *J. Phys. Chem. A* **1999**, *103*, 8375−8383.
(23) Burland, D. M.; Miller, R. D.; Walsh C. A. *Chem. Rev.* **1994**, *94*, 31−75.

two crystals have not been observed, and our calculated values are only an estimation. Generally, the observed average refractive index of borate compounds is from about 1.50 to 1.70 in a low-frequency zone.[24] Given the approximations involved in the computational model used here, the calculated average refractive indices of the two orthoborates seem to be underestimations of about 10%.

4. Conclusions

In this work, the new orthoborates are reported in single-crystal structural determinations and synthetic procedures, and their cluster units $(LiMBO_3)_2$ are chosen to calculate the electronic structures and refractive indices of $LiMBO_3$ (M = Sr, Ba). Electronic structure calculations find the lower valence band derived from O 2s and B 2s orbitals whereas the upper valence band was formed by the bonding interactions between O 2p and B 2p orbitals; electronic structure calculations find the lower conduction band derived from metal ionic orbitals whereas the upper conduction band was formed by the antibonding interactions between O and B valence orbitals. The closer to the top of the valence band, the more contributions from the O 2p orbitals; the closer to the top of the conduction band, the more contributions from the B valence orbitals. The charge transfer from O 2p orbitals to cationic orbitals is found to make significant contributions to the calculated refractive index of these compounds, and the refractive index is larger for $LiSrBO_3$ than for $LiBaBO_3$.

Acknowledgment. This investigation was supported by the national Science Foundation of China (29973048) and the Foundation of State Key Laboratory of Structural Chemistry (200027).

CM000808I

(24) Davis, H. M.; Knight, M. A. *J. Am. Ceram. Soc.* **1945**, *28*, 97−102.